Hindawi
Advances in Civil Engineering
Volume 2018, Article ID 5784831, 15 pages
https://doi.org/10.1155/2018/5784831

Research Article

Experimental Study on Physicomechanical Properties of Sandstone under Acidic Environment

Shuguang Li,[1] **Runke Huo**,[1] **Bo Wang**,[1] **Zhenzhong Ren**,[1] **Yu Ding**,[2] **Meiting Qian**,[1] **and Tian Qiu**[1]

[1]*School of Civil Engineering, Xi'an University of Architecture and Technology, Xi'an 710055, China*
[2]*School of Civil and Resource Engineering, University of Science and Technology Beijing, Beijing 100083, China*

Correspondence should be addressed to Runke Huo; huorkdq@xauat.edu.cn

Received 28 December 2017; Revised 20 March 2018; Accepted 5 April 2018; Published 2 May 2018

Academic Editor: Xiang Fan

The influence of acid solution and immersion time on the physicomechanical properties of sandstone is investigated. Uniaxial compression tests on sandstone samples are conducted to determine the variations of relative mass, deformation, and strength characteristics of sandstone subjected to different pH sulfuric acid corrosion values. The changes of pH and Mg^{2+} and Ca^{2+} concentration of immersion solutions are monitored during soaking. The corrosion mechanism of sandstone attacked by the acid solution is discussed with the results of SEM tests. Based on the nondestructive CT scanning test, the damage variables of acid-corroded sandstone are deduced, and the damage degree of sandstone is quantitatively analyzed. The results indicate that the deformation characteristics of sandstone samples under acid attack are characterized by the softening of rock, and the softening degree gradually increases with the increase of the acidity and the soaking time. The peak strength of sandstone samples declines as soaking time extends. The chemical effects lead to a large amount of dissolution of the rock mineral assemblage, resulting in the large-scale development of the pores inside the rock, which changes the macroscopic mechanical properties. The damage variables of acid corrosion sandstone based on CT numbers are deduced, and the quantitative relationship between damage variables and immersion time is established, which provides a basis for constructing a damage constitutive model of sandstone in the acidic environment.

1. Introduction

With the deterioration of environmental pollution, acid deposition has a serious impact on human activities. Acid rain, one of the main products of acid deposition, has various influences on the physical, chemical, and mechanical properties of rock materials. The deterioration of rock properties caused by acid rock interaction is a slow chemical process, which leads to the change of the mineral composition, microstructure, and mechanical properties of rock, resulting in poor engineering effects.

In recent years, many achievements have been made in the research on the influence of acidic environment on the physical and mechanical properties of rocks. Chen et al. [1] had carried out microscopic mechanical tests on the uniaxial compression fracture process of rocks under chemical corrosion, discussed the corrosion effect of different chemical solutions on uniaxial compression strength of rocks, and analyzed the microfracture characteristics and corrosion mechanism of rock under chemical etching. By simulating the indoor corrosion test under acidic environment, Huo et al. [2, 3] studied the degradation of physicomechanical properties and established the constitutive model of acid-corroded sandstone and sandstone-like materials. Xu et al. [4] and Li et al. [5] had carried out shear strength tests of sandstones subjected to different water chemical solution erosion. The mechanism of chemical damage of sandstone was discussed, and the relationship between porosity and shear strength was established. The influence of hydrochemical corrosion on the sandstone destruction, crack opening, and expansion direction was obtained. Chen et al. [6], Ding et al. [7], Han et al. [8], and Gao et al. [9] had performed the physical and

mechanical tests on the chemical corrosion and freeze-thaw cycles of granite, limestone, sandstone, and red sandstone, respectively. Physical and mechanical damage laws of rock under the combined action of the freeze-thaw cycle and water chemical solution were analyzed. Wang et al. [10, 11] and Han et al. [12] had studied the effect of chemical solution soaking on mechanical properties of sandstone by uniaxial and triaxial compression tests. They found that the mechanical properties of sandstone decrease obviously after chemical corrosion, and it is closely related to the change of porosity. The conclusion was drawn that the elastic modulus and compressive strength decrease with the increase of immersion time and acidity. Through a series of core tests, He and Guo [13] studied the failure of rock strength affected by different acid solutions from macroscopic and microscopic perspectives. Zhang [14] had investigated the macro- and mesodamage characteristics of argillaceous sandstone under dry-wet cycles in acidic condition. The influence of dry-wet cycles and the acid solution on the mechanical parameters of argillaceous sandstone was analyzed. Ding et al. [15] had studied the mechanical damage characteristics and chemical dissolution behaviour of limestone under different chemical solutions. A time-dependent corrosion equation of uniaxial compressive strength of limestone was developed under various chemical solutions. Chemical dynamic erosion equations of limestone were developed. Xie et al. [16] had carried out conventional triaxial and rheological tests on natural limestone and chemically etched porous limestone, respectively. They analyzed the effects of chemical corrosion on the pore-changing and aged mechanical properties of limestone. Currently, the study of microscopic damage to rock by CT nondestructive testing technology is gradually emerging [17, 18]. Yang et al. [19] applied the CT detection technique for the study of rock damage characteristics, established a mathematical model of CT number distribution in damaged rock, and deduced a formula for expressing the rock damage variables by CT numbers. Liu et al. [20, 21] used the digital image processing technique to analyze the CT images of rocks under different temperatures, achieved the pseudocolour enhancement and histogram analysis of the frozen rock CT images, and completed the digital representation of the frozen rock ice content, frozen water content, and damage information. Through the full-section CT scanning test of three sandstone with different initial microstructure, Fu et al. [22] investigated the evolution mechanism of the microscopic damage of the rock samples under the action of the wet-dry cycles and obtained the damage evolution equation of sandstone.

Reviewing the literature, the current research results mainly focus on the influence of chemical solution on macroscopic mechanical properties of rocks, lacking researches on the influence of accelerated corrosion on rock physicomechanical properties for a long time, and the rock damage analysis based on CT digital image processing is still rare. Against this background, in this paper, the common sandstone in water conservancy and civil engineering is taken as the research object. Based on the uniaxial compression test, the macroscopic mechanical properties of sandstone under acidic environment are systematically studied. The mechanism of acid rock interaction is discussed by SEM tests and the change of Mg^{2+} and Ca^{2+} concentration of immersion solutions. The damage variables of acid corrosion sandstone based on CT numbers are deduced, and the quantitative relationship between damage variables and immersion time is established, which provides a basis for constructing the damage constitutive model of sandstone in the acidic environment.

Table 1: Debris components and contents.

Cutting composition	Content (%)
Quartz	58
Feldspar	11
Calcite	5
Mica	3
Chlorite	1
Siliceous cuttings	6
Limestone cuttings	2
Cement	7
Clay	3
Heavy minerals	Occasionally

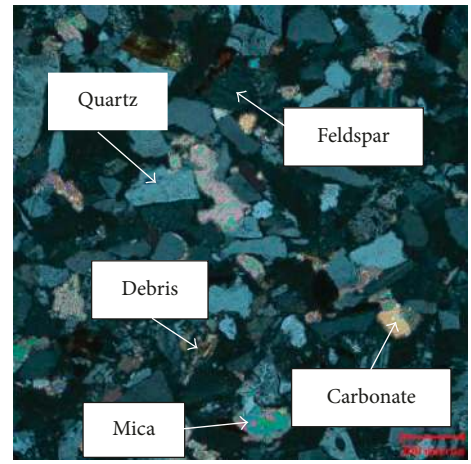

Figure 1: Microscope image of the sandstone sample.

2. Experimental Program

2.1. Materials. The sandstone specimens used in the tests were sampled from the water conservancy project in Shanxi Province, China, where the sandstone samples have high homogeneity and integrity. The X-ray diffraction test identified that the name of the sandstone is green-grey fine-grained calcareous feldspar sandstone. Table 1 summarizes the main features. Figure 1 shows the microstructure of the sandstone sample.

The sample was processed into a cylinder with a diameter of 50 mm and a height of 100 mm, and the basic dimensions and machining accuracy were in line with Standard for Tests Method of Engineering Rock Masses [23]. Before the test, the samples were sonic tested. The specimens with a large difference in wave velocity were excluded, and the sandstone samples were grouped according to the longitudinal wave velocity. A total of 28 sandstone specimens were selected and divided into three groups. Grouping and soaking of the sandstone samples are shown in Table 2.

Table 2: Debris components and contents.

Group number	Immersion state	Sample number	Wave velocity range (m/s)	Mass range (g)
1	Natural	#1~4	2467~2775	529.67~534.8
2	pH = 1 H_2SO_4	#5~16	2416~2477	523.93~533.08
3	pH = 3 H_2SO_4	#17~28	2941~2973	522.69~528.92

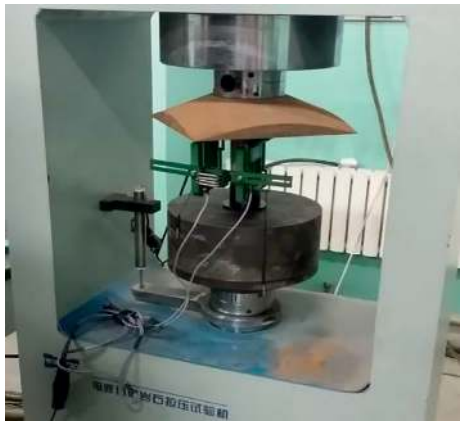

Figure 2: Uniaxial compression test.

Figure 3: SEM test.

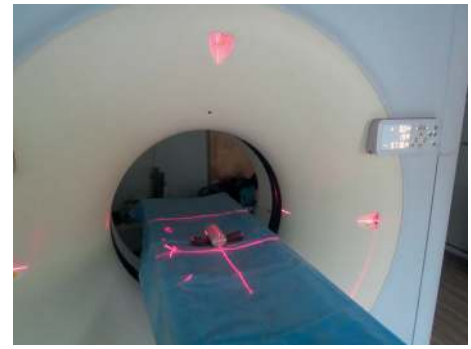

Figure 4: CT test.

2.2. Test Methods. In this paper, pH = 1 and 3 sulfuric acid solutions (H_2SO_4) were used to simulate the acidic environment. The sandstone specimens were immersed and etched at room temperature and atmospheric pressure. The experiment was divided into six phases, every 30 days for one phase. To observe the significant changes of the corroded sandstone samples in a relatively short period, the immersion solution was renewed every 30 days during the test (no change of the type and pH of the replacement solution). Before soaking in the solutions, the samples were photographed, and the initial mass of the samples was weighed (Figure 2). Then, the samples were placed in the configured two kinds of solution. A reagent bottle with a volume of 3 L was used to avoid evaporation. The pH and ion concentration of Mg^{2+} and Ca^{2+} of the solution and the mass of the samples were measured periodically. Uniaxial compression strength following GB/T50266-2013 [23] of the specimens after being subjected to acid attack was tested at 30, 90, and 180 days. SEM and CT scanning tests were conducted on the sandstone samples at the same time.

2.3. Test Apparatus. The pH test equipment and ion concentration test equipment used in the experiment are Leica PHS-3C and Metrohm 792 Basic IC, respectively. The weighing instrument is electronic balance JA12002 with a dividing value of 0.01 g. The oven is WGL-30B with a temperature range of room temperature plus 5~300°C. The uniaxial compression tests were conducted in a LETRY electrohydraulic rock pressure testing machine (Figure 2). The maximum axial load was 1500 kN. Japan JSM-7500F electron microscope equipment (Figure 3) was used to obtain SEM images of the samples. Philips Brilliance 16 spiral CT machine (Figure 4) was used to obtain the CT images of the samples.

3. Results and Discussion

3.1. Change Law of pH Values of the Soaking Solution. The variation curves of the pH values of the soaking solution in different stages are shown in Figures 5(a) and 5(b). It is observed in the figures that the pH values of the soaking solution show an increasing trend first and then tend to be stable with the lengthening of soaking time. The acidity of the soaking solution becomes balanced gradually in the process of rock being acidified. The pH value of the soaking solution increased rapidly in the initial soaking period (0~15 d), which increased to 2.85 and 4.22 at the first stage for sulfuric acid solutions with pH = 1 and 3, respectively, indicating that the chemical reaction between the samples and acid solution is fierce during the first 15 days of immersion. With the increase of immersion time and lengthening of the infiltration path, the pH value of the solution increased gradually and then tended to be stable, indicating that sulfuric acid had visible time effect on the chemical corrosion of sandstone. For the different acid soaking

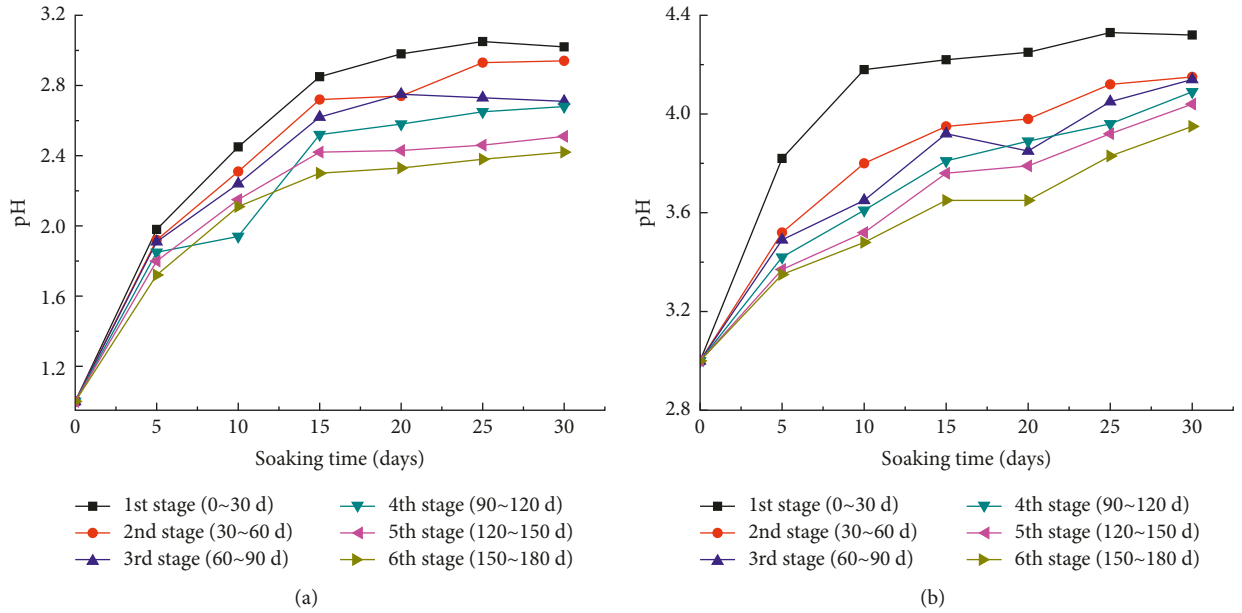

Figure 5: Variation curves of the pH values of sulfuric acid solution with time: (a) pH = 1 and (b) pH = 3.

Table 3: Mass change of the sandstone samples soaked in acid solution.

T (days)			0	30	60	90	120	150	180
pH = 1 H_2SO_4	Sample #6	m (wet)	529.60	539.42	538.36	537.42	536.62	536.09	535.54
		m (dry)		528.32	527.28	526.29	525.52	524.96	524.52
	Sample #11	m (wet)	530.25	540.04	539.07	538.12	537.27	536.79	536.13
		m (dry)		529.01	527.87	526.96	526.09	525.56	525.17
	Sample #15	m (wet)	532.42	542.33	541.17	540.23	539.48	538.89	538.45
		m (dry)		531.10	530.13	529.06	528.38	527.79	527.30
		$\overline{W}$ (%)		0.241	0.438	0.625	0.771	0.876	0.959
		$\overline{M}$ (%)		1.854	1.654	1.476	1.325	1.225	1.121
pH = 3 H_2SO_4	Sample #18	m (wet)	530.34	538.93	538.24	537.58	537.02	536.48	536.01
		m (dry)		529.45	528.82	528.13	527.54	526.98	526.58
	Sample #22	m (wet)	531.16	539.73	539.05	538.46	537.91	537.26	536.98
		m (dry)		530.23	529.70	528.94	528.27	527.75	527.41
	Sample #26	m (wet)	532.48	541.13	540.43	539.69	539.12	538.68	538.03
		m (dry)		531.63	530.89	530.26	529.74	529.14	528.68
		$\overline{W}$ (%)		0.167	0.286	0.416	0.527	0.633	0.708
		$\overline{M}$ (%)		1.619	1.489	1.365	1.259	1.157	1.069

solution, the change law of pH in each stage is the same. It can be seen from the growth of the pH value that the smaller the pH value of the initial solution (the stronger the acidity), the more severe the chemical reaction of acid rock, the greater the change in the pH value.

3.2. Change Law of Masses of Sandstone Samples. During soaking, the samples were taken out from the solution every 10 days, and the surface water of the samples was wiped off with a cotton cloth, and then the samples were left in the air for 5 minutes to ensure that the liquid is volatilized and dried. They were weighed in an electronic scale and the values were recorded; after that, they were kept in an oven for drying (24 h, 105°C), and then they were taken out and weighed. The mass of some of the samples is shown in Table 3.

To analyze the variation of sample mass quantitatively, mass change rate of the acid-corroded sandstone sample is defined as follows:

$$M = \frac{M_0 - M_t}{M_0} \times 100\%, \quad W = \frac{M_{ts} - M_0}{M_0} \times 100\%, \tag{1}$$

where M and W are the mass change rates of the dry samples and wet samples, respectively; M_0, M_t, and M_{ts} are the weight of the samples in natural, weight of the dry samples after soaking for t days, and weight of the wet samples after soaking for t days, respectively.

The variation curves of the relative mass change rate of the sandstone samples before and after drying are shown in

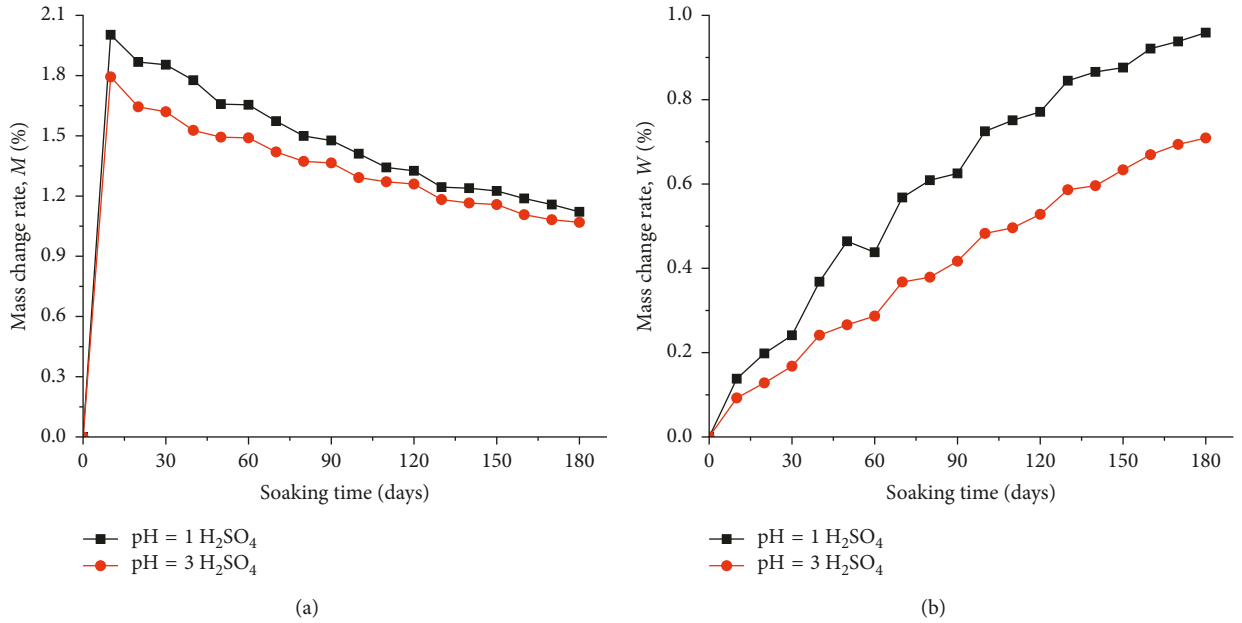

Figure 6: Mass change rate curves of the sandstone samples in different pH solutions: (a) wet samples and (b) dry samples.

Figures 6(a) and 6(b). As observed in the figures, the relative mass change rate of the samples soaked in different pH solutions shows different changing rules with prolonging the soaking time. The relative mass change rate of the wet samples soaked in the sulfuric acid solution with pH = 1 and 3 increases rapidly at the initial soaking time (0~15 d) and then decreases gradually with the increase of soaking time (Figure 6(a)). This shows that the diffusion of the solution is dominant during the initial reaction of acid rock reaction, and the mass of the sample increases due to water absorption. With the samples gradually saturated, the chemical corrosion plays a dominant role. The sandstone mineral components are hydrolyzed and dissolved, and the mass of the samples decreases. However, the relative mass change rate of the dry samples shows an increasing trend with the extension of soaking time (Figure 6(b)), and the smaller the pH, the greater the mass change rate of the dry samples. This means that the concentration of H^+ in the soaking solution is the main factor that determines the chemical reaction rate. The higher the concentration of H^+, the more the mineral components of the sample dissolved and the greater the mass loss.

In the first three soaking stages (0~90 d), the mass change rate of the dry samples increases significantly during the first 15 days of each stage (30 d) and then gradually slows down (Figure 6(b)). The mass change rate of the wet samples decreases significantly during the first 15 days of each stage and then slows down gradually (Figure 6(a)). In the last three soaking stages (90~180 d), the mass change rate of samples tends to be stable gradually. Experimental observation showed that a large number of bubbles generated in sulfuric acid solution with pH = 1 after 15 days of each soaking stage, and then floccule is gradually generated around the samples. However, only some bubbles formed in pH = 3 sulfuric acid solution, and no floccule is produced (Figure 7). The above analysis shows that the acid rock reaction is severe at each early stage (the first 15 days) and then tends to be stable over time.

3.3. Analysis of Mechanical Properties of Sandstone in the Acidic Environment

3.3.1. Influence of Acidic Environment on Deformation Characteristics of Sandstone. The sandstone samples were taken out after 30, 90, and 180 days of immersion in the acid solution for the uniaxial compression test. The tests are performed under a displacement-controlled mode with the loading rate set at 0.002 mm/s. The test results and stress-strain curves are shown in Table 4 and Figure 8, respectively. As can be seen from Figure 8, the stress-strain curve of sandstone can be divided into the following four stages: compaction stage, elastic stage, plastic stage, and failure stage.

(1) Compaction Stage. As can be seen from Figure 8 that the concave length of the natural specimen is short and the degree of deformation is small, it enters the elastic phase quickly. However, the compression stage of the sample attacked by acid solution increases obviously. Under the same immersion time, the compaction stage of the acid-corroded sandstone samples increased obviously, and the degree of depression gradually increased with the decrease of the pH values of the soaking solution. Under the same soaking solution, the compaction stage of the sample increased obviously, and the compaction point strain increased significantly with the soaking time prolonging. It shows that with the increase of acidity of the soaking solution and the prolongation of immersion time, the pore development in sandstone becomes more significant due to the dissolution of mineral particles,

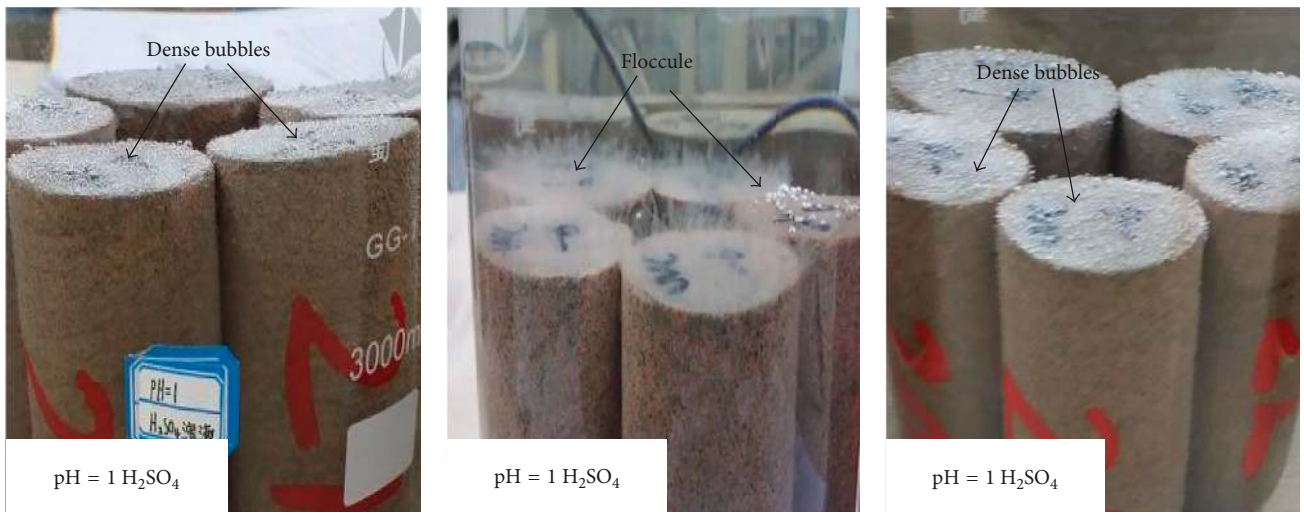

Figure 7: Experimental phenomenon of the samples in different pH solutions after soaking for 15 days.

Table 4: Uniaxial compressive test results of the sandstone samples subjected to acid corrosion.

Sample state	Soak solution	Peak intensity, σ_c (MPa)	$(\sigma_n - \sigma_c)/\sigma_n \times 100\%$ (%)	Axial strain at peak point, ε_c (10^{-3})	$(\varepsilon_c - \varepsilon_n)/\varepsilon_n \times 100\%$ (%)	Elastic modulus, E (GPa)	$(E_n - E)/E_n \times 100\%$ (%)
Natural		88.25		4.03		17.83	
Soaking for 30 days	pH = 1 H_2SO_4	58.14	34.12	5.38	33.50	12.42	30.37
	pH = 3 H_2SO_4	61.29	30.55	5.09	26.30	13.55	24.03
Soaking for 90 days	pH = 1 H_2SO_4	47.06	46.67	13.01	222.83	8.49	52.37
	pH = 3 H_2SO_4	57.67	34.65	10.63	163.77	10.82	39.30
Soaking for 180 days	pH = 1 H_2SO_4	34.28	61.16	21.02	421.59	3.36	81.17
	pH = 3 H_2SO_4	54.39	38.37	13.17	226.80	4.61	74.17

and the compaction stage of the stress-strain curve is more obvious.

(2) Elastic Stage. With the increase of axial pressure, the rock samples enter the elastic stage from the compaction stage. At this stage, the slope of the straight line segment is the elastic modulus E, and the smaller the E value, the more obvious the softening phenomenon of the rock sample subjected to acid corrosion. As can be seen from Table 4, the elastic modulus of the acid corrosion sandstone samples decreases to varying degrees compared with the natural state samples. The elastic modulus of the sandstone sample changes obviously under the action of different pH solutions, and the smaller the pH value of the solution, the larger the elastic modulus change. After soaking for 180 days, the elastic modulus of the sandstone samples subjected to acid solutions decreased significantly. The average value of the elastic modulus of the samples under the action of the sulfuric acid solution with pH = 3 reduced from 17.83 to 3.36 GPa, decreased by 74.17%. The average value of the elastic modulus of the samples subjected to the sulfuric acid solution with pH = 1 lowered from 17.83 to 4.61 GPa, decreased by 81.17%. The above analysis shows that the enhancement of acidity and the extension of soaking time will make the chemical reaction of acid and rock more thoroughly, and the softening effect of acid corrosion is more apparent.

(3) Plastic Stage. As can be seen from Figure 8, the plastic deformation stage of the sample is not obvious. The peak point strain of the plastic deformation stage reflects the deformation amount when the sandstone is damaged, and the greater the deformation, the greater the degree of softening of the sandstone by acid corrosion. The axial strain value of the peak point of the sandstone samples corroded by acid solution can be seen from Table 4. Figures 9(a) and 9(b) show the change rule of the axial strain of the peak point of the samples with the pH value of the soaking solution and soaking time, respectively. As can be seen from Figure 9(a)

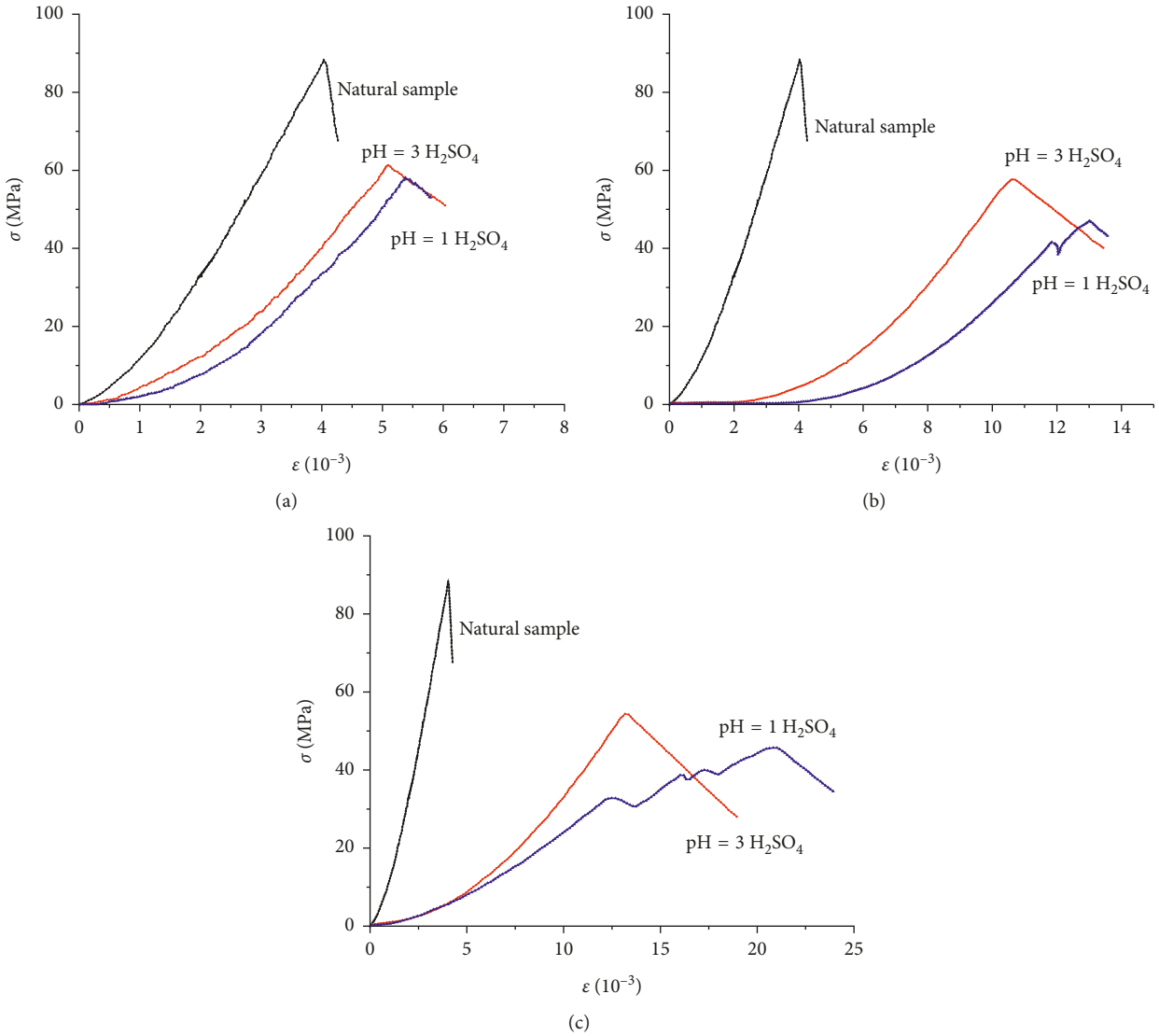

Figure 8: Uniaxial compressive stress-strain curves for the sandstone samples attacked by acid solutions for different soaking days: (a) 30 days, (b) 90 days, and (c) 180 days.

and Table 4, the axial strain of the peak point of the samples increases gradually with the increase of the acidity of the chemical solution at the same soaking time. As can be seen from Figure 9(b) and Table 4, the axial strain of the peak point of the rock sample corroded by acid also tends to increase with the immersion time. After 180 days of soaking, the peak point strain of the sample in the sulfuric acid solution with pH = 1 and 3 was multiplied by 5.216 and 3.268 times, respectively, than that of the sample in the natural state.

As can be seen from Figure 9 and Table 4, with the increase of acidity and immersion time, the uniaxial compressive strength of the acid-corroded sandstone specimen decreases, and the axial strain of the peak point increases. This indicates that the deformation characteristics of the sandstone samples under acid attack are characterized by the softening of rock, and the softening degree gradually increases with the increase of the acidity and the soaking time.

(4) Destruction Phase. Because of the strong brittleness of the sandstone samples, the destruction of the sandstone samples was often accompanied by a crisp sound, and the stress dropped rapidly after the failure of the samples, so the postpeak stage has not been obtained.

3.3.2. Influence of Acidic Environment on Strength Characteristics of Sandstone. As can be seen from Table 4, the peak strength of the samples in the natural state is the largest, which is 88.25 MPa, and the peak strength of the samples decreases after the acid attack. After soaking for 30, 90, and 180 days, the peak strength of the sandstone samples subjected to sulfuric acid solution with pH = 1 decreased by 34.12%, 46.67%, and 61.16%, respectively, and the peak strength of the sandstone samples subjected to sulfuric acid solution with pH = 3 decreased by 30.55%, 34.65%, and 38.37%, respectively. The analysis shows that the peak

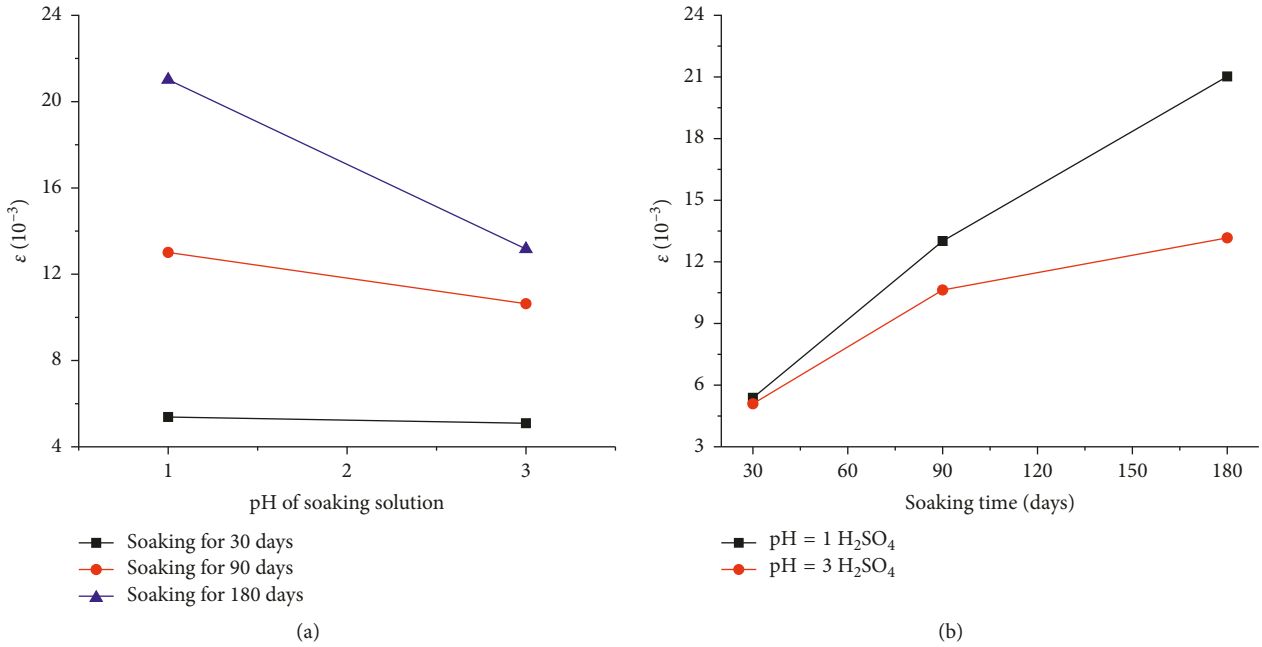

Figure 9: Relationships between axial peak strains of samples and (a) pH of solutions and (b) immersion time.

strength of the sandstone samples decreases with the increase of immersion time and solution acidity, and the degradation effect of peak strength is more obvious in a strong acid solution.

4. Study on Acid Corrosion Mechanism of Sandstone

4.1. Chemical Reaction Mechanism of Acid and Sandstone Samples. The change of macroscopic mechanical properties of the sandstone samples subjected to the acid solution is the result of the change of internal microstructure. At the initial stage of soaking, the chemical reaction between acid and rocks is mainly the ion exchange between H^+ and mineral components, which lead to the replacement of the cations of mineral crystals and the dissolution and deterioration of mineral components. With the depletion of H^+, the chemical reaction between the acid and rock gradually transforms into mineral hydrolysis, and the reaction rate slows down. The solubility of clay mineral in the acidic solution will also be greatly increased. Feldspar solubility in the acidic solution will greatly increase, and the solubility increases with the decrease of pH. The corrosion degree of calcite, dolomite, and other carbonate minerals increased significantly at normal pressure and temperature. The dissolution reaction equation is as follows:

$$\mathrm{CaMg(CO_3)_2\,(Dolomite)} + 4\mathrm{H^+} \rightarrow \mathrm{Ca^{2+}} + \mathrm{Mg^{2+}} + \mathrm{H_2O} + \mathrm{CO_2}\uparrow \quad (2)$$

$$\mathrm{CaCO_3\,(Calcite)} + 2\mathrm{H^+} \rightarrow \mathrm{Ca^{2+}} + \mathrm{H_2O} + \mathrm{CO_2}\uparrow \quad (3)$$

It can be seen from the above reaction mechanism that the chemical reaction between sulfuric acid and sandstone samples produces cations such as Ca^{2+} and Mg^{2+}. To analyze the dissolution rate of Mg^{2+} and Ca^{2+} in the soaking solution quantitatively, which is defined as the ratio of the variation of cation concentration and corrosion time after every ten days of immersion, the following formula is used:

$$A = \frac{C_t - C_0}{\Delta t} \cdot V, \quad (4)$$

where C_0 is the initial concentration of cation (mg/L), C_t is the concentration of cation after soaking t days (mg/L), V is the volume of the soaking solution (L), and Δt is the time difference before and after corrosion reaction (d).

As observed in Figure 10, the dissolution rates of Mg^{2+} and Ca^{2+} in two soaking sssolutions showed large change at the initial soaking stage (0~15 days) and then gradually decreased with the increase of soaking time. Under the same conditions, the smaller the pH value of the soaking solution, the higher the rate of cation dissolution. For example, the maximum dissolution rate of Ca^{2+} in the sulfuric acid solution with pH = 1 is 8.07 mg/d, which is 1.36 times that of the sulfuric acid solution with pH = 3. The dissolution rates of Mg^{2+} and Ca^{2+} in two different solutions at each soaking stage (30 days) were the same. The dissolution rate of cation in the initial immersion stage was higher and then decreased gradually. Moreover, in the same soaking solution and immersion stage, the dissolution rate of Ca^{2+} is larger than Mg^{2+}, which is the result of reaction of calcite and other calcium fillings with the acid solution.

4.2. Microstructure Changes of Sandstone Samples before and after Acid Attack. The acid-corroded sandstone samples were magnified 2000 times by scanning electron microscopy (SEM). The SEM images of the samples attacked by sulfuric acid solution (pH = 3 and 1) and the SEM images of natural sandstone samples are shown in Figures 11 and 12.

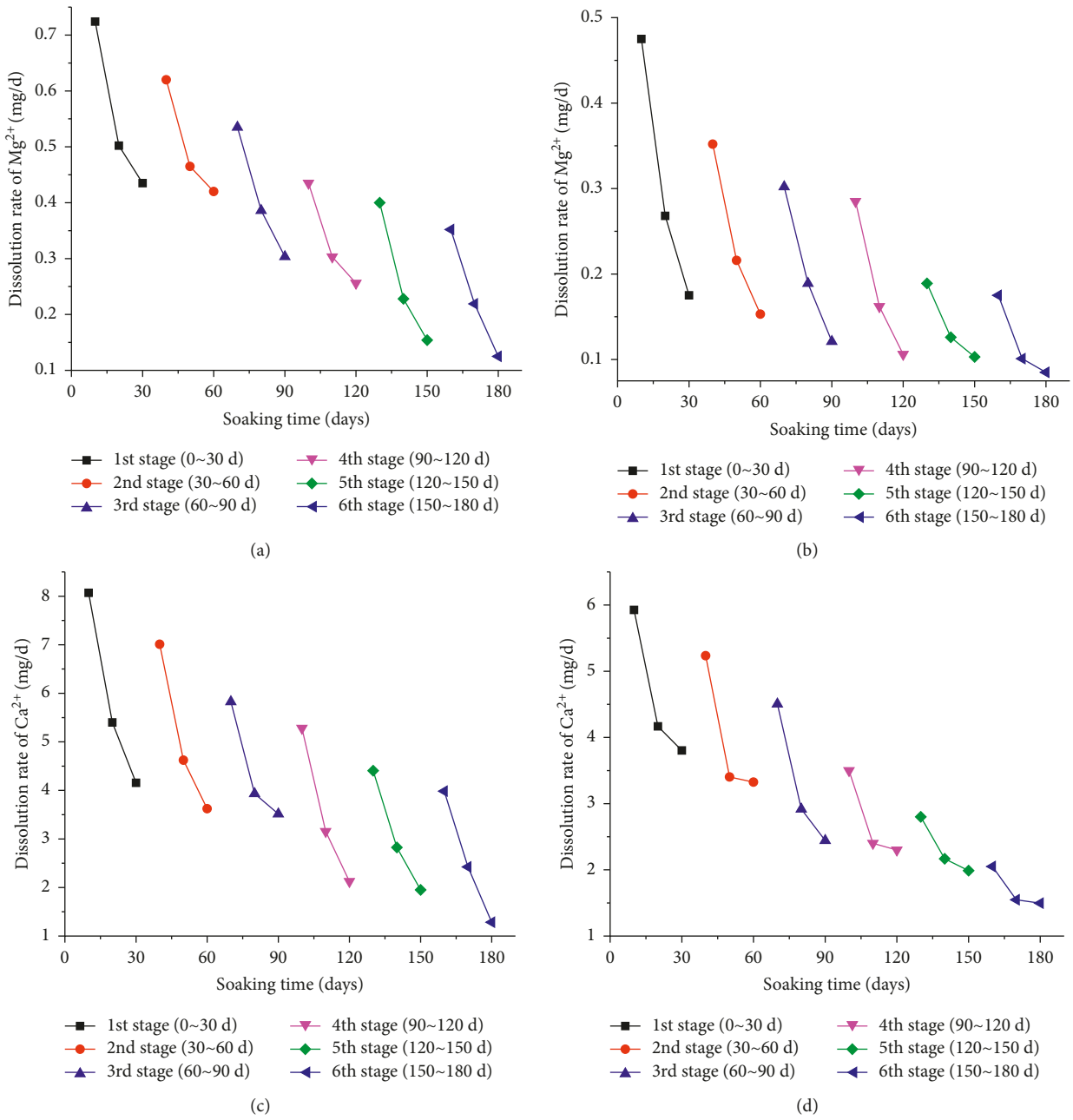

FIGURE 10: Cation dissolution rate diagram of soaking solution. Dissolution rate of Mg^{2+} in H_2SO_4 solution at (a) pH = 1 and (b) pH = 3. Dissolution rate of Ca^{2+} in H_2SO_4 solution at (c) pH = 1 and (d) pH = 3.

As can be seen from Figures 11(a) and 12(a), in the natural state, the mineral crystals of sandstone are mostly irregular flake-like or lump-like, and the mineral particles are disorderly distributed without apparent directionality. The mineral particles are in point-like or linear contact with each other, and the pores and fissures of the sample are developed. The SEM images of the sandstone samples soaked in the pH = 3 sulfuric acid solution for 30 days (Figure 11(b)) show that the surface of the mineral crystal becomes rough due to the dissolution. The interlayer cementing materials of the sandstone samples are dissolved, and the lamellar crystals are decomposed after the acid attack. When soaked for 90 days (Figure 11(c)), the surface of the mineral crystals becomes rougher, the original large-size crystal particles in the form of flakes and blocks no longer exist, and the dissolution holes appear on the surface of the crystals, which make the rock pores increase. Compared with the pH = 3 sulfuric acid solution, the SEM images of the sandstone samples attacked by the pH = 1 sulfuric acid solution (Figures 12(b) and 12(c)) show that the microstructure change is more visible. Especially after soaking for 90 days (Figure 12(c)), the dissolution degree of mineral particles is severe, the cementation degree between particles is worse, the initial microcracks are fully developed, and the penetration of

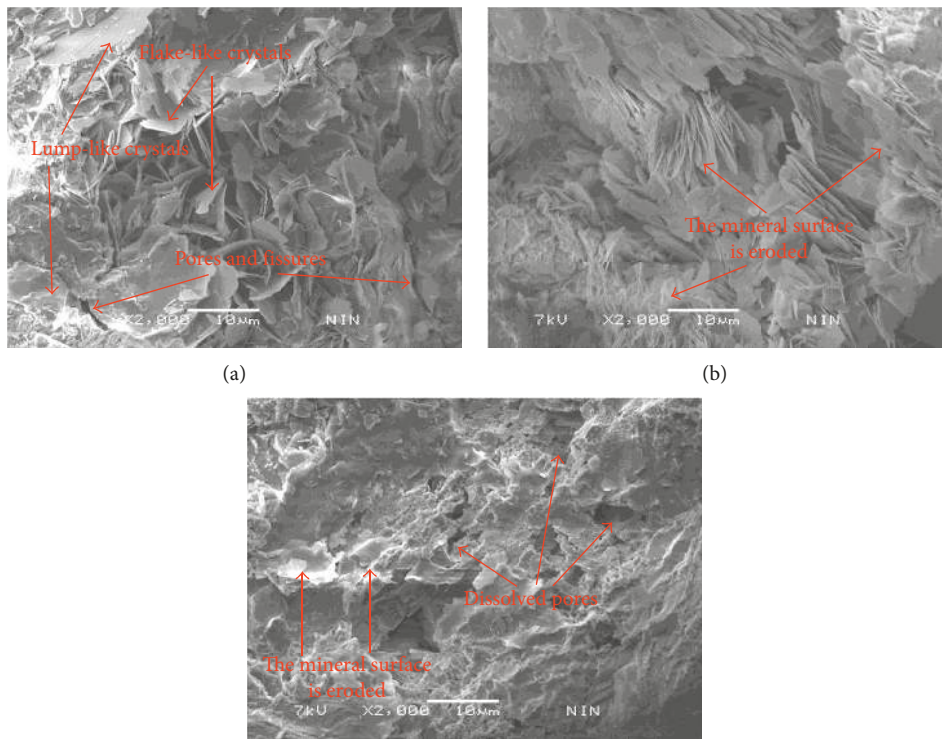

(a) (b) (c)

Figure 11: SEM images of the sandstone samples attacked by pH = 3 H_2SO_4 solution. (a) Natural sandstone sample. Sandstone samples soaked in sulfuric acid solution at pH = 3 for (b) 30 days and (c) 90 days.

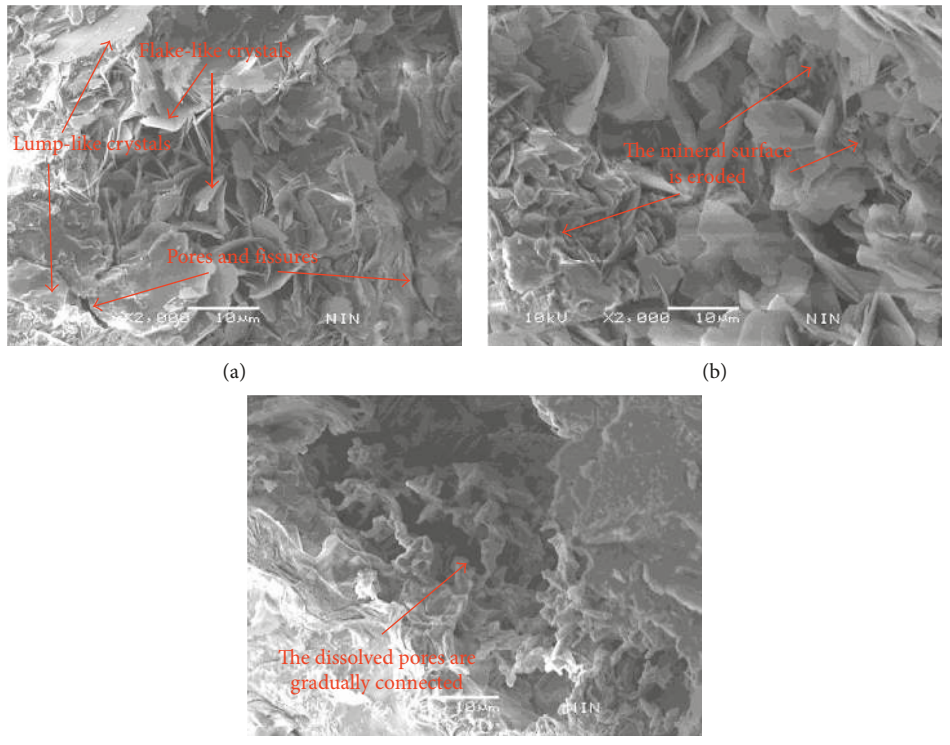

(a) (b) (c)

Figure 12: SEM images of the sandstone samples attacked by pH = 1 H_2SO_4 solution. (a) Natural sandstone sample. Soaking in pH = 1 sulfuric acid solution for (b) 30 days and (c) 90 days.

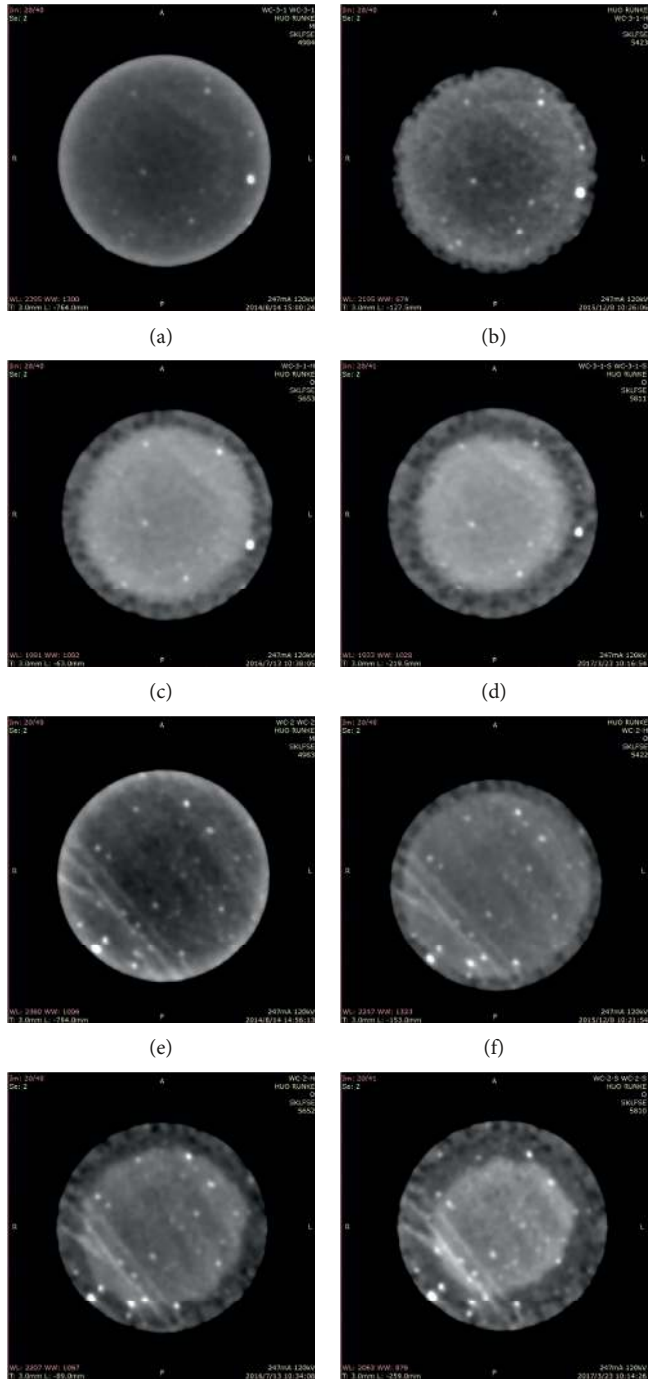

(a) (b) (c) (d) (e) (f) (g) (h)

Figure 13: CT images of the middle layer of the sandstone specimens subjected to sulfuric acid solution with different pH values for different stages. (a) pH = 3 H_2SO_4 (0 day), (b) pH = 3 H_2SO_4 (30 days), (c) pH = 3 H_2SO_4 (90 days), (d) pH = 3 H_2SO_4 (180 days), (e) pH = 1 H_2SO_4 (0 day), (f) pH = 1 H_2SO_4 (30 days), (g) pH = 1 H_2SO_4 (90 days), and (h) pH = 1 H_2SO_4 (180 days).

many small holes increases the connectivity of the porosity of the specimen, thus forming a loose granular skeleton structure.

The above analysis shows that after the sandstone samples are corroded by sulfuric acid, the mineral aggregates and cement of the samples are dissolved and destroyed, the particle size of mineral particles decreases, and the secondary pores and fissures of the samples develop obviously. This results in changes in the mechanical properties of the sandstone samples.

5. Quantitative Calculation of Acid-Corroded Sandstone Damage

Figure 13 shows the CT scanning images of the middle layer of the sandstone samples in different stages immersed in two

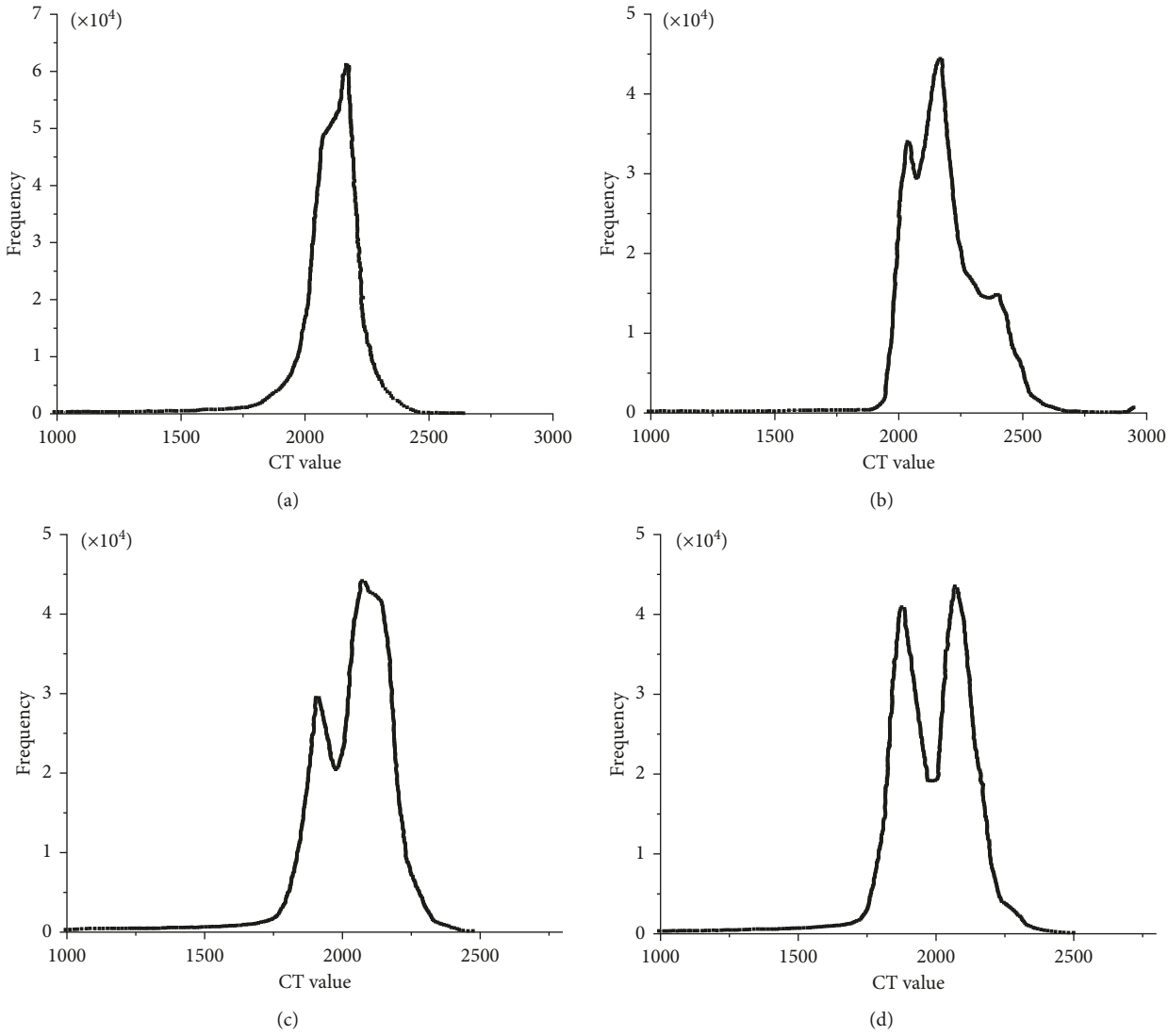

Figure 14: CT number distribution diagram of the sandstone specimens attacked by sulfuric acid solution (pH = 1) for (a) 0 day, (b) 30 days, (c) 90 days, and (d) 180 days.

different pH solutions. It can be seen from Figure 13 that the damage of the sandstone samples is obviously different when immersed in the sulfuric acid solution at different pH values for different periods of time, and the smaller the pH value of the solution, the more serious the acid corrosion of the sandstone samples. The middle layer CT scanning images of the sandstone specimen in different soaking stages (0, 30, 90, and 180 days) of the pH = 1 sulfuric acid solution are selected. The CT value frequency distribution curves of the samples are obtained by MATLAB based on the CT histogram technique, which is shown in Figure 14. As can be seen from Figure 14, the peak shape of the frequency curve of the CT value of the natural sandstone specimen showed a unimodal distribution, which begins to appear a bimodal distribution after 30 days of being acid-etched. With the extension of the etching time, the second peak increases gradually, and the peak difference gradually decreases. Indicating that the damage of sandstone is not only the original damage caused by material defect after acid corrosion but also hollow damage caused by dissolution of mineral particles. With the extension of corrosion time, these damages become more and more dominant.

The damage variable, as a measure of the damage degree of the rock, indicates the decrease of the effective bearing area of the rock sample due to the defects such as microcracks in the process of corrosion damage. The initial damage characteristics of sandstone are the unimodal distribution [19] of CT numbers (Figure 14(a)). After being acid-etched, the distribution of the CT number is bimodal distribution (Figures 14(b)–14(d)). The damage variable formula based on the bimodal distribution of CT numbers has been deduced [19]. Then, the following assumptions [24] are deduced to derive the formula of rock material damage variables based on the bimodal distribution of CT numbers:

(1) The damage in the rock appears as holes, and the holes are distributed randomly in the rock.

(2) The area of one single hole in that CT resolution unit is approximately equal, and v_0 is used as the area of the hole.

(3) The number of voids is independent of each other in mutually intersecting areas.

(4) The probability that there are h holes in the body-centred T domain is only related to t, not related to T, and not constant to 1.

(5) There are only a limited number of holes in the finite area T, that is, $\sum_{k=0}^{\infty} p_h(t) = 1$.

(6) The probability of appearing for one hole in the area t is the higher order infinitesimal about T, that is, $\lim_{t\to 0}(1 - P_0(t) - P_1(t))/t = 0$.

For the rock material whose CT frequency curve is unimodal distribution, supposing the area of CT resolution unit is t, the probability that the number n of holes in the area t is k can be proved by the assumptions (2)–(5):

$$P(n = k) = e^{-\lambda t}\frac{(\lambda t)^k}{k!}, \tag{5}$$

where λ is the mathematical expectation of the number of holes per unit area.

If the density of nondestructive rock material is ρ_0 and the number of holes in the resolution unit is n, the average density distribution in the resolution unit can be written as follows:

$$\rho = \rho_0\left(1 - n\frac{v_0}{v}\right). \tag{6}$$

For different resolution units, the distribution in (6) is given by (5), and the expectation and variance of formula (6) are obtained as follows:

$$\begin{aligned} E(\rho) &= \rho_0(1 - \lambda v_0), \\ D(\rho) &= \rho_0^2\frac{v_0^2}{t}\lambda, \end{aligned} \tag{7}$$

where the $E(\rho)$ and $D(\rho)$ represent mathematical expectation and variance, respectively, and the above two formulas can be used to solve the problem of void area v_0 and void density λ as follows:

$$\begin{aligned} v_0 &= \frac{D(\rho)t}{\rho_0(\rho_0 - E(\rho))}, \\ \lambda &= \frac{(\rho_0 - E(\rho))^2}{D(\rho)t}. \end{aligned} \tag{8}$$

For v_0 and λ within the unit area only, the damage variable on the corresponding scan section is as follows:

$$D = \frac{S - S_1}{S} = \frac{S_2}{S} = \frac{Av_0\lambda t}{S}, \tag{9}$$

Table 5: Damage variables of the intermediate scanning layer of the sandstone samples at different time intervals in different solutions.

Solution type	Soaking time (days)	Damage variable (D)
pH = 3 H_2SO_4	30	0.1596
	60	0.2189
	90	0.2703
	120	0.3112
	150	0.3475
	180	0.3698
pH = 1 H_2SO_4	30	0.2032
	60	0.3098
	90	0.3792
	120	0.4207
	150	0.4813
	180	0.5372

where S is the cross-sectional area of rock scanning, S_1 is the effective area of the scanning section, S_2 is the defect area of the scanning section damage, A is that number of resolution units in the scan section, and t is the area of the resolution unit.

If the resolution of the CT device is w, then $t = w^2$ and $A = S/w^2$, and D can be obtained as follows:

$$D = \lambda v_0 = 1 - \frac{E(\rho)}{\rho_0}. \tag{10}$$

There are two types of damage in rock materials with the bimodal distribution of CT numbers: damage caused by material defects (characteristic distribution parameters are λ_1 and v_{01}) and void damage caused by dissolution of mineral particles (characteristic distribution parameters are λ_2 and v_{02}). The damage variable based on the bimodal distribution of CT numbers can be written as follows:

$$D = \frac{1}{2}(D_1 + D_2) = 1 - \frac{E(\rho_1) + E(\rho_2)}{2\rho_0}. \tag{11}$$

The relationship between CT number and rock density is known from [19] as follows:

$$\rho = \frac{1000 + H}{1000 + H_r}\rho_r, \tag{12}$$

where H is the CT number of the damaged sandstone, H_r is the CT number of the sandstone matrix material, and ρ_r is the density of the sandstone matrix material.

Equations (11) and (12) can solve the damage variables of the scanned cross section of acid-eroded sandstone based on the CT number. The calculated damage variables at different corrosion stages of the middle scanning layer of the sandstone samples attacked by the sulfuric acid solution with pH = 3 and 1 are shown in Table 5. It can be seen from Table 5 that the chemical damage of the sandstone samples in different soaking stages is different. With the increase of acidity and corrosion time, the damage variable of the sandstone samples shows an increasing trend, and the stronger the acidity, the bigger the increase of the damage variable.

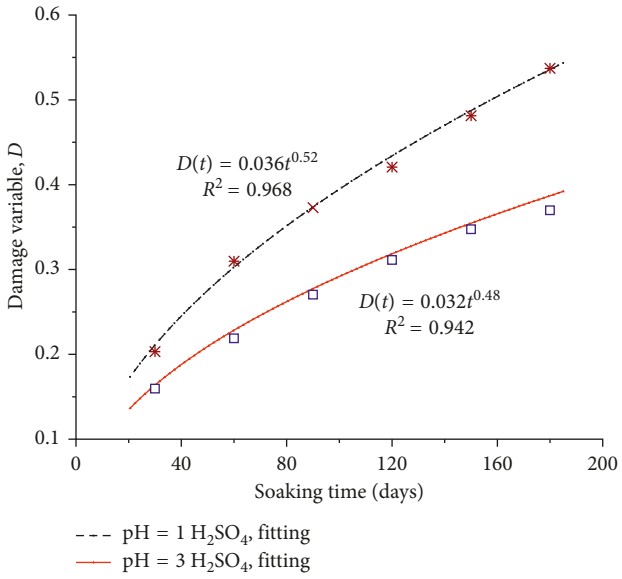

Figure 15: Relationship between the damage variables of the sandstone samples and immersion time under different pH sulfuric acid solutions.

Fitting the damage variables can obtain the relationship between the damage variable of acid-corroded sandstone and the soaking time (Figure 15):

$$\begin{aligned} &\text{pH} = 3\ \text{H}_2\text{SO}_4\text{:}\ D(t) = 0.032t^{0.48}\left(R^2 = 0.942\right), \\ &\text{pH} = 1\ \text{H}_2\text{SO}_4\text{:}\ D(t) = 0.036t^{0.52}\left(R^2 = 0.968\right). \end{aligned} \tag{13}$$

Therefore, the damage variables of acid-corroded sandstone can be expressed as

$$D(t) = \alpha t^{\beta}, \tag{14}$$

where α and β are the chemical influence coefficients, which are related to the type of acid and the pH value.

6. Conclusions

Based on the results of this study, the following conclusions can be drawn:

(1) Under the acidic environment, the pH value of the immersion solution and the mass change of the sandstone samples have phased characteristics. The pH value of the solution increased rapidly at the initial stage of each immersion phase (15 days) and tended to be stable gradually with the prolongation of soaking time. The mass change rate of the wet sandstone samples increased rapidly in the first 15 days of soaking and then gradually decreased and stabilized. The mass change rate of the dry sandstone samples shows a tendency of increase during the entire corrosion stage, and its growth rate gradually decreased and stabilized.

(2) With the prolongation of immersion time and the increase of solution acidity, the compaction phase of the sandstone samples became longer, the elastic phase became shorter, the axial strain of the peak point increases, and the softening degree of the sandstone samples enhances gradually. Compared with the natural state, the acidic environment has an apparent effect on the mechanical deterioration of sandstone. The peak intensity of sandstone after attacking 180 days by the sulfuric acid solution with pH = 1 and 3 decreased by 61.16% and 38.37%, respectively.

(3) The action of the acid solution can not only dissolve interlayer cement of sandstone but also dissolve and decompose the large-size mineral aggregates, which leads to the large-scale development of the pores in the rock and changes its macroscopic mechanical properties.

(4) Based on the bimodal distribution of CT value histogram, the damage variables of sandstone in the acidic environment are deduced. The quantitative relationship between damage variable and corrosion time is established, which provides a basis for constructing the damage constitutive model of sandstone subjected to acid corrosion.

Conflicts of Interest

The authors declare that they have no conflicts of interest.

Acknowledgments

The authors would like to thank the National Natural Science Foundation of China (41172237) for supporting this research project.

References

[1] S. L. Chen, X. T. Feng, and S. J. Li, "Effects of chemical erosion on uniaxial compressive strength and meso-fracturing behaviors of rock," *Journal of Rock Mechanics and Engineering*, vol. 22, no. 4, pp. 547–551, 2003.

[2] R. K. Huo, *Experimental Research on Progressive and Deteriorative Characteristics of Sandstone and Mortar Materials Subjected to Hydrochloric Acid Corrosion*, Ph.D. thesis, Xi'an University of Technology, Xi'an, China, 2006.

[3] R. K. Huo, J. Li, H. W. Xin, and B. Wang, *Regularity Analysis on Corrosion Progressive and Physical-Chemical Characteristic of Sandstone Subjected to Acid Rain*, Xi'an University of Architecture and Technology, Xi'an, China, 2016.

[4] J. Xu, H. Wu, L. Z. Cheng, J. Liu, and W. J. Zhou, "Experimental study of shearing failure properties of sandstone under acidic conditions," *Chinese Journal of Rock Mechanics and Engineering*, vol. 31, no. S2, pp. 3898–3903, 2012.

[5] P. Li, J. Liu, G. H. Li, J. B. Zhu, and S. G. Liu, "Experimental study for shear strength characteristics of sandstone under water-rock interaction effects," *Rock and Soil Mechanics*, vol. 32, no. 2, pp. 380–386, 2011.

[6] Y. L. Chen, P. Wang, X. W. Zhang, and X. Du, "Experimental research on mechanical properties of granite in chemical dissolution under freeze-thaw cycles," *Chinese Journal of Geotechnical Engineering*, vol. 36, no. 12, pp. 2227–2235, 2014.

[7] W. X. Ding, T. Xu, H. Y. Wang, and J. P. Chen, "Experimental study of mechanical property of limestone under coupled

chemical solution and freeze-thaw process," *Chinese Journal of Rock Mechanics and Engineering*, vol. 34, no. 5, pp. 979–985, 2015.

[8] T. L. Han, J. P. Shi, and X. S. Cao, "Fracturing and damage to sandstone under coupling effects of chemical corrosion and freeze-thaw cycles," *Rock Mechanics and Rock Engineering*, vol. 49, no. 11, pp. 4245–4255, 2016.

[9] F. Gao, Q. L. Wang, H. W. Deng, J. Zhang, W. G. Tian, and B. Ke, "Coupled effects of chemical environments and freeze-thaw cycles on damage characteristics of red sandstone," *Bulletin of Engineering Geology and the Environment*, vol. 76, no. 4, pp. 1481–1490, 2016.

[10] W. Wang, X. H. Li, Q. Z. Zhu, C. Shi, and W. Y. Xu, "Experimental study of mechanical characteristics of sandy slate under chemical corrosion," *Rock and Soil Mechanics*, vol. 38, no. 9, pp. 2559–2573, 2017.

[11] W. Wang, T. G. Liu, and J. F. Shao, "Effects of acid solution on the mechanical behavior of sandstone," *Journal of Materials in Civil Engineering*, vol. 28, no. 1, pp. 409–420, 2016.

[12] T. L. Han, Y. S. Chen, J. P. Shi, Z. Yu, and M. M. He, "Experimental study of mechanical characteristics of sandstone subjected to hydrochemical erosion," *Chinese Journal of Rock Mechanics and Engineering*, vol. 32, no. S2, pp. 3065–3072, 2013.

[13] C. M. He and J. C. Guo, "Study on the mechanism of the effect of acid on the mechanical properties of limestone," *Journal of Rock Mechanics and Engineering*, vol. 32, no. S2, pp. 3016–3021, 2013.

[14] L. Zhang, *Study on Macro-Meso Damage Characteristics of Argillaceous Sandstone under Dry-Wet Cycle in Acidic Condition*, Ph.D. thesis, Chongqing University, Chongqing, China, 2014.

[15] W. X. Ding, J. P. Chen, T. Xu, H. J. Chen, and H. Y. Wang, "Mechanical and chemical characteristics of limestone during chemical erosion," *Rock and Soil Mechanics*, vol. 36, no. 7, pp. 1825–1830, 2015.

[16] S. Y. Xie, J. F. Shao, and W. Y. Xu, "Influences of chemical degradation on mechanical behaviour of a limestone," *International Journal of Rock Mechanics and Mining Sciences*, vol. 48, no. 5, pp. 741–747, 2011.

[17] T. S. Ma, C. H. Yang, P. Chen, X. D. Wang, and Y. T. Guo, "On the damage constitutive model for hydrated shale CT using scanning technology," *Journal of Natural Gas Science and Engineering*, vol. 28, pp. 204–214, 2016.

[18] T. S. Ma and P. Chen, "Study of meso-damage characteristics of shale hydration based on CT scanning technology," *Petroleum Exploration and Development*, vol. 41, no. 2, pp. 249–256, 2014.

[19] G. S. Yang, D. Y. Xie, and C. Q. Zang, "The quantitative analysis of distribution regulation of CT values of rock damage," *Chinese Journal of Rock Mechanics and Engineering*, vol. 17, no. 3, pp. 279–285, 1998.

[20] H. Liu, G. S. Yang, W. J. Ye, Y. J. Shen, and L. Y. Tang, "Analysis of unfrozen water content and damage characteristics based on histogram technique of CT images," *Journal of Glaciology and Geocryology*, vol. 37, no. 6, pp. 1591–1598, 2015.

[21] H. Liu, G. S. Yang, W. J. Ye, and Y. J. Shen, "Analysis of ice content and damage characteristics of frozen rock based on pseudo-color enhanced CT image," *Chinese Journal of Underground Space and Engineering*, vol. 12, no. 4, pp. 912–919, 2016.

[22] Y. Fu, Z. J. Wang, X. R. Liu et al., "Meso damage evolution characteristics and macro degradation of sandstone under wetting-drying cycles," *Chinese Journal of Geotechnical Engineering*, vol. 12, no. 4, pp. 1653–1661, 2017.

[23] GB/T50266-2013, *Standard for Tests Method of Engineering Rock Masses*, China Planning Press, Beijing, China, 2013.

[24] H. H. Yu and W. Yang, "CT identification of hole damage," *Mechanics in Engineering*, vol. 15, no. 6, pp. 41–45, 1993.